Exhibit 21

LIMNOLOGY and OCEANOGRAPHY

ASLO

Limnol. Oceanogr. , 2018, 1–19

doi: 10.1002/lno.10823

Season-specific trends and linkages of nitrogen and oxygen cycles in Chesapeake Bay

Jeremy M. Testa ,*[1] **W. Michael Kemp,**[2] **Walter R. Boynton**[1]

[1]Chesapeake Biological Laboratory, University of Maryland Center for Environmental Science, Solomons, Maryland
[2]Horn Point Laboratory, University of Maryland Center for Environmental Science, Cambridge, Maryland

Abstract

A three-decade time series of solute concentrations was combined with a box-modeling system to analyze long-term trends in the concentration, production, and transport of dissolved inorganic nitrogen species along the mainstem axis of Chesapeake Bay. Water- and salt-balance calculations associated with box-modeling provided regional, seasonal, and interannual estimates of net advective and nonadvective transport and net biogeochemical production rates for oxygen and dissolved nitrogen. The strongest decadal trends were observed for decreasing late-summer ammonium concentrations in bottom layers from brackish to polyhaline bay regions. Contemporaneous trends of increasing late-summer bottom-layer dissolved oxygen (O_2) concentration were consistent with the observed NH_4^+ patterns, suggesting that increasing dissolved O_2 levels may also reflect declining bottom respiration and drive nitrogen loss via increased rates of coupled nitrification–denitrification. Significant (but weaker) trends of increasing nitrate plus nitrite (NO_{2+3}^-) concentration and net production were consistent with the notion that increased nitrification may be stimulated by increasing dissolved O_2 concentrations. Sorting bottom water NH_4^+ and NO_{2+3}^- net production rates into two pools (before and after the year 2000) revealed that general seasonal patterns were similar, but recent NH_4^+ net production rates were consistently lower and NO_{2+3}^- and NO_2^- rates higher in summer and fall compared to earlier years, especially in the middle Bay regions. We conclude that late-season replenishment of oxygen associated with declining nutrient loads induced a negative feedback process, whereby decreased hypoxia suppressed NH_4^+ recycling and created conditions favorable for additional nitrogen loss via coupled nitrification–denitrification.

Many estuaries, lagoons, and coastal systems have undergone anthropogenic eutrophication, which is generally linked to increasing nutrient (particularly nitrogen) inputs (e.g., Howarth and Marino 2006; Paerl et al. 2006) from watershed and/or atmospheric sources (Nixon 1995; Cloern 2001). A common manifestation of nutrient enrichment is the enhancement of organic carbon production, which upon degradation causes depletion of oxygen from bottom waters in stratified estuarine ecosystems. This leads to loss of habitat for many benthic or demersal organisms and radical shifts in ecologically important biogeochemical cycles. These conditions of seasonal "hypoxia" (dissolved oxygen < 62.5 μM) reflect a globally significant and expanding degradation of coastal ecosystem health (Díaz and Rosenberg 2008). Although eutrophication trends have been described for a number of coastal ecosystems, time-series data documenting trajectories of recovery are far less common (Kemp et al. 2009), but with a growing number of examples (Greening and Janicki 2006; Riemann et al. 2016). Consequently, general theoretical trajectories of degradation and recovery are poorly corroborated (Duarte et al. 2009).

Most analyses linking hypoxia and eutrophication have focused on how increased nutrient levels stimulate algal growth and accumulation of labile organic carbon that stimulates bottom water and sediment respiration and associated O_2 depletion, but the full biogeochemical responses to nutrient enrichment are more complex (Rabalais et al. 2014). Seasonally stratified eutrophic systems are characterized by oxidized photic surface waters with net photosynthetic production of O_2 and rapid air-sea exchange to replenish any O_2 deficiencies or surpluses. In contrast, the bottom water and sediments are characterized by low dissolved O_2 and chemically reduced conditions with active anaerobic respiratory pathways, including sulfate and nitrate reduction that generate large pools of the reduced metabolites sulfide and ammonium, respectively (Conley et al. 2002). Sulfide accumulates under anoxic conditions and tends to react with iron and manganese to form solid-phase compounds that are reoxidized to sulfate later in

*Correspondence: jtesta@umces.edu

the fall when dissolved O_2 becomes available due to vertical mixing of the water column (Cornwell and Sampou 1995). In contrast, ammonium is either oxidized to nitrate in the sulfide-sensitive (Joye and Hollibaugh 1995) process of nitrification that directly consumes O_2, or it is transported to the upper, photic surface layer where it eventually could support O_2 depletion by stimulating algal growth, organic matter sinking, and bottom water respiration. In the former case, nitrate produced by nitrification drives denitrification and related process that shunt fixed nitrogen salts to gaseous forms unavailable to support algal growth. Recent studies show that low-dissolved O_2 conditions favor ammonium recycling over denitrification, thus creating a system-level positive feedback process whereby, greater hypoxia leads to larger pools of ammonium (as percentage of total nitrogen [TN] loading), which leads to greater O_2 consumption and more hypoxia (Testa and Kemp 2012).

Many temperate estuaries, like Chesapeake Bay, are particularly susceptible to nutrient loading effects on organic production and oxygen depletion because of their relatively long water residence times, stratified water columns, and deep channels flanked by productive shallows (Kemp et al. 2005). At the same time, shallow estuarine environments like Chesapeake Bay are particularly susceptible to changes in circulation and mixing due to wind stress and tidal forcing (e.g., Wilson et al. 2008; Scully 2010) that can either replenish bottom water oxygen or exacerbate hypoxia. Seasonally hypoxic conditions have been documented for the Potomac River tributary since 1912 (Sale and Skinner 1917) and for the mainstem of Chesapeake Bay since the 1930s (Newcombe and Horne 1938). In general, the summer volume of hypoxic water had increased from the mid-1950s through the mid-1980s, when it leveled and began a gradual late-summer decline starting around 1990 and continuing to the present decade (Hagy et al. 2004; Murphy et al. 2011). Analysis of time-series data for nutrients and oxygen revealed that late-summer hypoxia in the estuary has declined slowly ($\sim$ 1% yr^{-1}) following gradual reductions in nitrogen loading for two decades. In fact, late-summer hypoxia volume has been highly correlated with nitrogen loading for the last several decades, whereas the early summer extent of hypoxic water is more weakly correlated with annual nitrogen inputs and has been related to physical factors, such as stratification (Murphy et al. 2011). In addition, recent studies have suggested that the duration of seasonal hypoxia in Chesapeake Bay has been declining during recent decades (Zhou et al. 2001), where the reductions in duration of hypoxic conditions have been attributable to progressively earlier termination of annual hypoxia (Murphy et al. 2011). Early termination of hypoxia has the potential to substantially alter nitrogen cycling in late summer and fall, which is a time when the oxidation of accumulated ammonium pools leads to an annually occurring, short-term burst in elevated nitrite and nitrate concentrations (McCarthy et al. 1984; Horrigan et al. 1990).

Analysis of time-series data from Chesapeake Bay monitoring has revealed many significant trends for key ecological properties in different regions of the estuary. For example, apart from hypoxia volume and duration discussed above, trends have been detected (1) for phytoplankton biomass and community composition (Harding and Perry 1997; Harding et al. 2015*a*), (2) for submersed aquatic vegetation areal cover and density (Orth et al. 2010; Gurbisz and Kemp 2014), and (3) for all eutrophication-relevant variables in small tributaries where substantial nutrient reductions have taken place (Boynton et al. 2014). Similar analyses in other large, eutrophic coastal systems (Andersen et al. 2015; Riemann et al. 2016) indicate that a wide-variety of estuaries have responded positively to nutrient loading reductions. Many of these trends have been found to correlate significantly with nutrient loading and/or climate-change drivers, and the majority of efforts have focused on concentrations of water-column constituents, as opposed to ecological or biogeochemical rates (e.g., Harding et al. 2015*b*; Riemann et al. 2016).

In the present study, we analyzed a long-term record of dissolved O_2 and nitrogen concentrations over three decades for surface and bottom layers of several regions along the longitudinal axis of the Chesapeake Bay mainstem. We aimed to address feedbacks between oxygen availability and nitrogen cycling and the extent to which these interactions have a regional and seasonal dependence that was related to long-term changes in the spatial and temporal extent of hypoxia. This approach addresses research questions of broad interest related to eutrophication of the coastal zone and its impacts on the coupled cycling of nitrogen, carbon, and dissolved O_2. We analyzed correlations and interactions between nitrogen and oxygen distributions using a diagnostic, salt- and water-balance computation to examine changes in the net transformation and transport of four key solutes (nitrate, nitrite, ammonium, and oxygen).

Methods

Study site

The Chesapeake Bay is a large estuary located in the mid-Atlantic coastal region of the United States. The estuary is $\sim$ 300-km long, has a mean low-water estuarine volume of 74.4 km^3, and a mean depth of 6.5 m (Fig. 1). A 20–30-m deep channel (1–4 km wide) runs the length of the middle region of the Bay, but is flanked by broad shallow (< 10 m) shoals to the east and west. Two-layered circulation occurs for most of the year in the estuary, driven by a mean freshwater input of 2300 m^3 s^{-1} from the Susquehanna River that induces a seaward-flowing surface layer and a landward-flowing bottom layer. The upper estuary (north of 39°N) is vertically well mixed. Salinity, temperature, dissolved O_2, chlorophyll *a* (Chl *a*), and nutrient concentrations have been monitored at 2–4 week intervals at 20 stations along the central axis of the main body of the estuary since 1985 (www.chesapeakebay.net; Fig. 1).

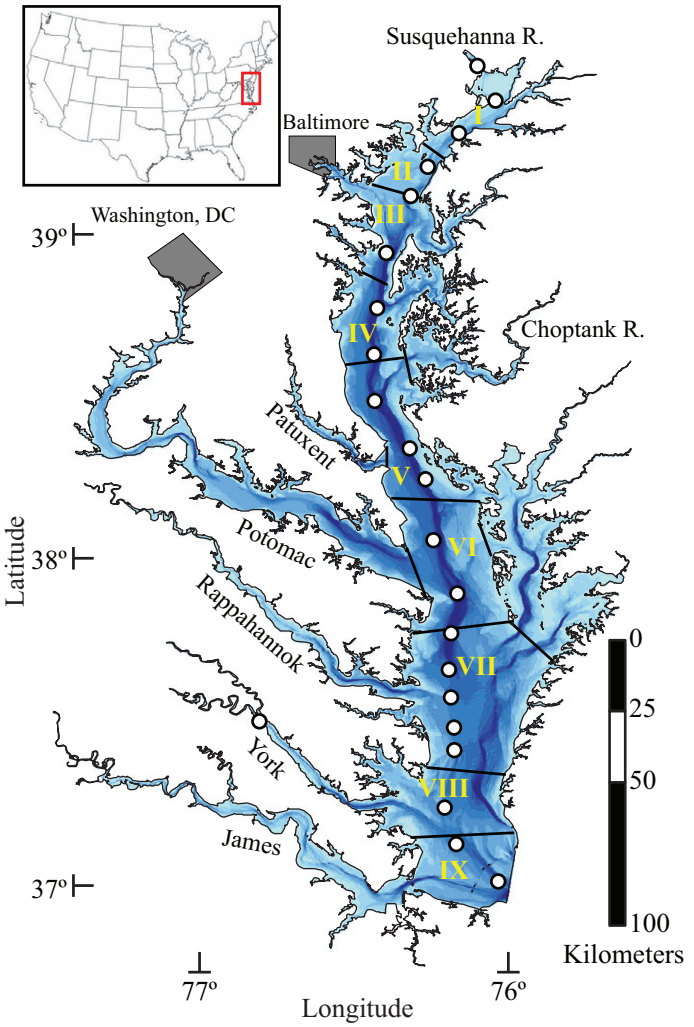

Fig. 1. Map of Chesapeake Bay, including boundaries of box-model regions (black lines), tributary rivers, and sampling stations used to generate mainstem Bay interpolations (white circles). Box numbers are included in yellow. For the James and York River estuaries, two rivers input freshwater (James = Appomattox and James; York = Pamunkey and Mattaponi). Blue shading indicates depth.

Computing salt and water transport

We computed the Chesapeake Bay's time-dependent, seasonal mean circulation using a box-model approach for the period 1985–2013. The box model equations and computations utilized in this analysis were developed, first applied, and presented for Chesapeake Bay by Hagy (2002). This box-modeling approach utilizes mean monthly salinity, volume, and freshwater input data and computes advective and nonadvective exchanges of water and salt between adjacent control volumes (which are assumed to be well mixed) and across end-member boundaries using the solution to nonsteady-state equations balancing salt and water inputs, outputs, and storage changes (Pritchard 1969; Officer 1980; Hagy et al. 2000). Stratified estuarine regions are represented by surface and bottom layers that capture the essential features of two-layered estuarine circulation (Pritchard 1969). The box model used in this analysis calculates advection and mixing between nine boxes in the mainstem of the Chesapeake estuary (Boxes 2–9 include surface and bottom-layer subboxes, Fig. 2). Boundaries separating adjacent boxes were defined based on data availability, degree of density stratification, and an effort to retain similar salinity gradients and water volumes among boxes. The salt and water balances (Eqs. 1 and 2, respectively) for a surface-layer box "m" in the two-layer scheme are described below:

$$V_{tm}\frac{ds_{tm}}{dt} + V_m\frac{ds_{tm}}{dt}V_{tm}\frac{ds_{tm}}{dt} = Q_{m-1}s_{m-1} + Qv_m s'_m - Q_m s_m + Ev_m(s'_m - s_m) + [E_{m-1,m}(s_{m-1} - s_m) + E_{m,m+1}(s_{m+1} - s_m)] \quad (1)$$

$$dV_m/dt = 0 = Q_{m-1} + Qv_m + Qf_m - Q_m \quad (2)$$

where, V_m is the volume of the box, Q_m and Q_{m-1} are the advective transports to the seaward box and from the landward box, Qv_m is the vertical advective input into the box, $E_{m-1,m}$ and $E_{m,m+1}$ are the nonadvective exchanges with the landward box and with the seaward box, Ev_m is the vertical nonadvective exchange, s_m and s'_m are the salinities in the upper and bottom-layer boxes, and s_{m-1} and s_{m+1} are the salinities in the landward and seaward boxes. Note the additional salt storage term associated with exchange of salt with the tributaries flanking the mainstem Bay ($V_{tm}\frac{ds_{tm}}{dt}$). For Eq. 2, Qf_m is the freshwater input directly into the box. The left-hand side of Eq. 1 is computed as the monthly salinity change, while the left-hand side of Eq. 2 is assumed to be zero at monthly time scales. The salt and water balances (Eqs. 3 and 4) for a bottom-layer box "m" in the 2D scheme are similar

$$V'_m\frac{ds'_m}{dt} = Q'_{m+1}s'_{m+1} - Qv_m s'_m - Q'_m s'_m - Ev_m(s'_m - s_m) \quad (3)$$

$$dV'_m/dt = 0 = Q'_{m+1} - Qv_m - Q'_m \quad (4)$$

where, Q'_m and Q'_{m+1} are the advective transports to the landward box and from the seaward box and s'_{m+1} is the salinity of the seaward box in the bottom layer.

Freshwater input

The Susquehanna River and six major tributary rivers are the dominant sources of freshwater to Chesapeake Bay (Fig. 1). The Susquehanna River is the largest freshwater source (62% of mean annual freshwater input) and enters directly into Chesapeake Bay, while several large tributary rivers contribute the majority of the remaining freshswater input, including the Choptank (0.2%), Patuxent (1%), Potomac (19%), Rappahannock (3%), York (3%), and James (13%) Rivers (Fig. 1; Zhang et al. 2015). Daily freshwater inputs from all rivers were measured since 1985 by the United States Geological Survey. The York River includes the combined flows of the Mattaponi and Pamunkey Rivers, whereas the James River

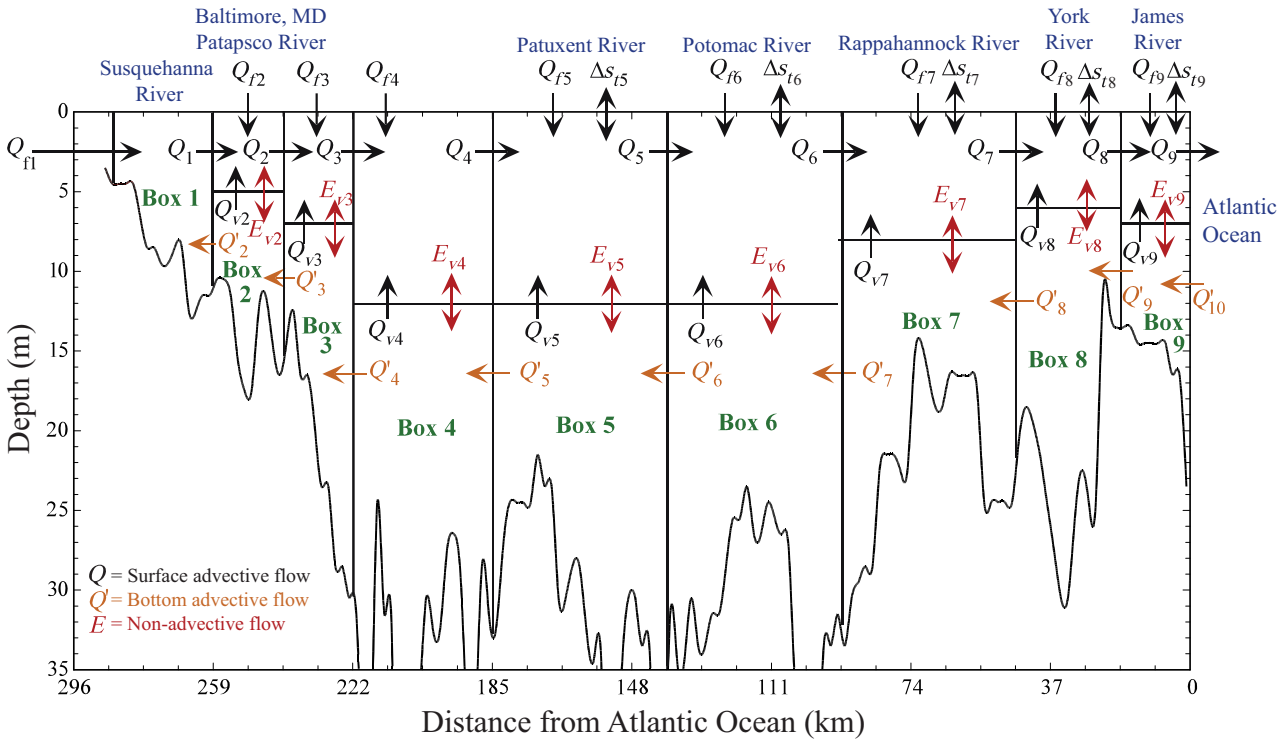

Fig. 2. Diagram of salt- and water-balance (box) model for Chesapeake Bay, including relevant freshwater inputs, transport coefficients, and box identifiers. In Box 5–9, Δs values represent salt exchanges between the boxes and adjacent, connected tributaries. An aerial view of this model is included in Fig. 1.

combines the James and Appomattox Rivers (Fig. 1). The drainage basins of the gauges at the fall lines of these rivers comprise 130,798 km^2, roughly 78% of the 166,717 km^2 drainage area of Chesapeake Bay. Ungauged portions of the lower watersheds of the six major tributaries were estimated on the basis of the flow/area of the associated tributary, but inputs from tributaries are highly processed before reaching the mainstem of Chesapeake Bay, leading to high-retention rates of dissolved and particulate materials within the tributaries (Boynton et al. 1995, 2008).

Nutrient and oxygen transport and production rates

We computed monthly and seasonal rates of transport and net biogeochemical production of dissolved O_2 and dissolved inorganic nitrogen for 17 regions of the Chesapeake estuary from 1985 to 2013. Physical transport rates for these nonconservative biogeochemical variables were computed by multiplying the solute concentration by the advective and nonadvective fluxes (*Q*s and *E*s, respectively) for each box and month. Rates were calculated for nitrate (NO_3^-), nitrite (NO_2^-), ammonium (NH_4^+), and dissolved O_2. Monthly mean values of these variables were computed for each box (and upstream and downstream boundaries) using monitoring data from 20 stations along the central axis of the Bay (Fig. 1). Monitoring cruises were conducted on a bi-weekly basis, except in the months of October to March, when cruises were conducted monthly, and concentration data were available from 1985 to 2014. The vertical resolution of the salinity and oxygen data is 1 m, while dissolved nitrogen data were sampled four to five times in a given vertical profile. Both mainstem and tributary data were interpolated to a grid transecting the estuary at a vertical resolution of one meter and a horizontal resolution of 1.8 km. Grid cells corresponded to tabulated cross-sectional volumes (Cronin and Pritchard 1975), which were used to compute volume-weighted average salinity and nutrient concentrations (Hagy et al. 2000).

Net biogeochemical production rates (P_m or P'_m = production − consumption) for each nonconservative water quality variable were computed for each box using the analytical solutions for the advective (*Q*) and nonadvective (*E*) transport rates in each box. The equations are similar in form to the salt balance (Eqs. 1 and 2), except salinity is replaced with the water quality variable and the net production term (P_m or P'_m) is added. Thus, for a surface-layer box "*m*" in the two-layer scheme of the box model without longitudinal *E*s, the mass balance equation is

$$V_m \frac{dc_m}{dt} = Q_{m-1}c_{m-1} + Qv_m c'_m + Ev_m(c'_m - c_m) - Q_m c_m + P_m \quad (5)$$

which can be rearranged to calculate P_m

$$P_m = V_m \frac{dc_m}{dt} - Q_{m-1}c_{m-1} - Qv_m c'_m - Ev_m(c'_m - c_m) + Q_m c_m \quad (6)$$

We assumed that $E_{m,m-1} = E_{m,m+1} = 0$ for all boxes, and $Ev_m = 0$ and $Qv_m = 0$ for $m = 1$ (Officer 1980; Hagy

Table 1. The dimensions, including the length, surface area, pycnocline area, cross-sectional area (CLA), volume of the surface layer and bottom layer Boxes 1–9 in Chesapeake Bay, and boundaries (*see* Fig. 1; adapted from Hagy 2002).

	Box 1	Box 2	Box 3	Box 4	Box 5	Box 6	Box 7	Box 8	Box 9
Length (km)	28	18	29	37	46	46	47	27	18
Surface area (km^2)	217	255	169	489	655	1025	1425	782	454
Pycnocline area (km^2)		80	92	144	249	278	904	510	289
Surface layer CLA (10^3 m^2)	28	60	52	107	123	185	212	178	139
Bottom layer CLA (10^3 m^2)		13	31	27	35	37	85	83	57
Surface layer volume (10^6 m^3)	773	1077	995	3961	5675	8502	9977	4796	2500
Bottom layer volume (10^6 m^3)		242	593	988	1612	1684	4015	2246	1018
Pycnocline depth (m)		5	7	12	12	12	8	7	6
Boundary (N, km from ocean)	287	259	241	222	185	139	93	46	19
Boundary (S, km from ocean)	259	241	222	185	139	93	46	19	1

et al. 2000). For any bottom-layer box "m," the mass balance expression is

$$V'_m \frac{dc'_m}{dt} = Q'_{m+1}c'_{m+1} - Qv_m c'_m - Q'_m c'm - Ev_m(c'_m - c_m) + P'_m \quad (7)$$

which can be rearranged to calculate bottom-layer net production, P'_m

$$P'_m = V'_m \frac{dc'_m}{dt} - Q'_{m+1}c'_{m+1} + Qv_m c'_m + Q'_m c'_m + Ev_m(c'_m - c_m) \quad (8)$$

where, c is the concentration of the nonconservative material and P_m and P'_m are the net production (or consumption) rates in the surface and bottom layers, calculated per unit area or volume using geometry data for each box (Table 1).

Box-model computations have clear advantages and disadvantages for analysis of estuarine biogeochemical data. Box models are imperfect tools, given the assumptions of fixed volumes, the aggregation to regionally- and seasonally averaged concentrations and circulation, and the dependence on statistical interpolation to generate box-averaged salinity and nutrient concentrations. These computations have many advantages, however, including the fact that they are data-driven, constrained by observations, yield estimates of physical circulation that are representative of mean Bay circulation, have compared well with direct in situ measurements (Hagy 2002) and serve as tools to identify processes of interest that are otherwise difficult and expensive to obtain at consistent time and space scales. The computation of volume-weighted concentrations in each box also provides a spatially integrated view of concentration, as opposed to single vertical profiles with a focus on surface and or bottom concentrations. These volume-weighted regional mean values capture changes in vertical distributions, aggregate over spatially correlated zones, and account for different habitats (e.g., shallow and deep waters).

Nutrient measurement methods

Improvements in analytical methodlogy have led to reductions in the detection limits for both NO_{2+3}^- and NH_4^+ measurements made during the period of this study. A complete description of the monitoring database, its methodology, and quality assurance practices are available on the Chesapeake Bay Program's web-based monitoring interface (https://www.chesapeakebay.net/what/downloads/cbp_water_quality_database_1984-present). We addressed the possibility that changes in detection limit could have biased our analysis by surveying the nutrient concentration data sets we used and identifying all instances where the reported concentration was at the detection limit (indicated by a "<" in the qualifier column of the Chesapeake Bay Program database). The instances of measurements made at the detection limit (0.7 μM and lower over time) were primarily limited to surface waters during summmer (for both NO_{2+3}^- and NH_4^+) and for bottom waters during winter (NH_4^+). In general, neither of these regions and times overlap with the late-summer period where we focused our analysis. For NO_{2+3}^-, any effect of a reduction in the detection limit would have led to increasingly smaller concentrations over time, where we observed the opposite pattern. NH_4^+ concentrations were at their seasonal peak in the mid summer, with concentrations well above historic and recent detection limits.

Results

We discovered a long-term decline in bottom water NH_4^+ concentrations in the late-summer and fall season that correlates with increases in dissolved O_2 and NO_{2+3}^- concentrations. These trends correspond to changes in the net biogeochemical production and net transport of NH_4^+ and NO_{2+3}^- that operate over seasonal and regional scales in Chesapeake Bay and other comparable estuaries (Cloern and Jassby 2010). The reductions in NH_4^+ and increases in dissolved O_2 also correspond to recent, but modest declines in nitrogen input from the Susquehanna River (Murphy et al. 2011; Zhang et al. 2015; Harding et al. 2015*b*; Testa et al. 2018).

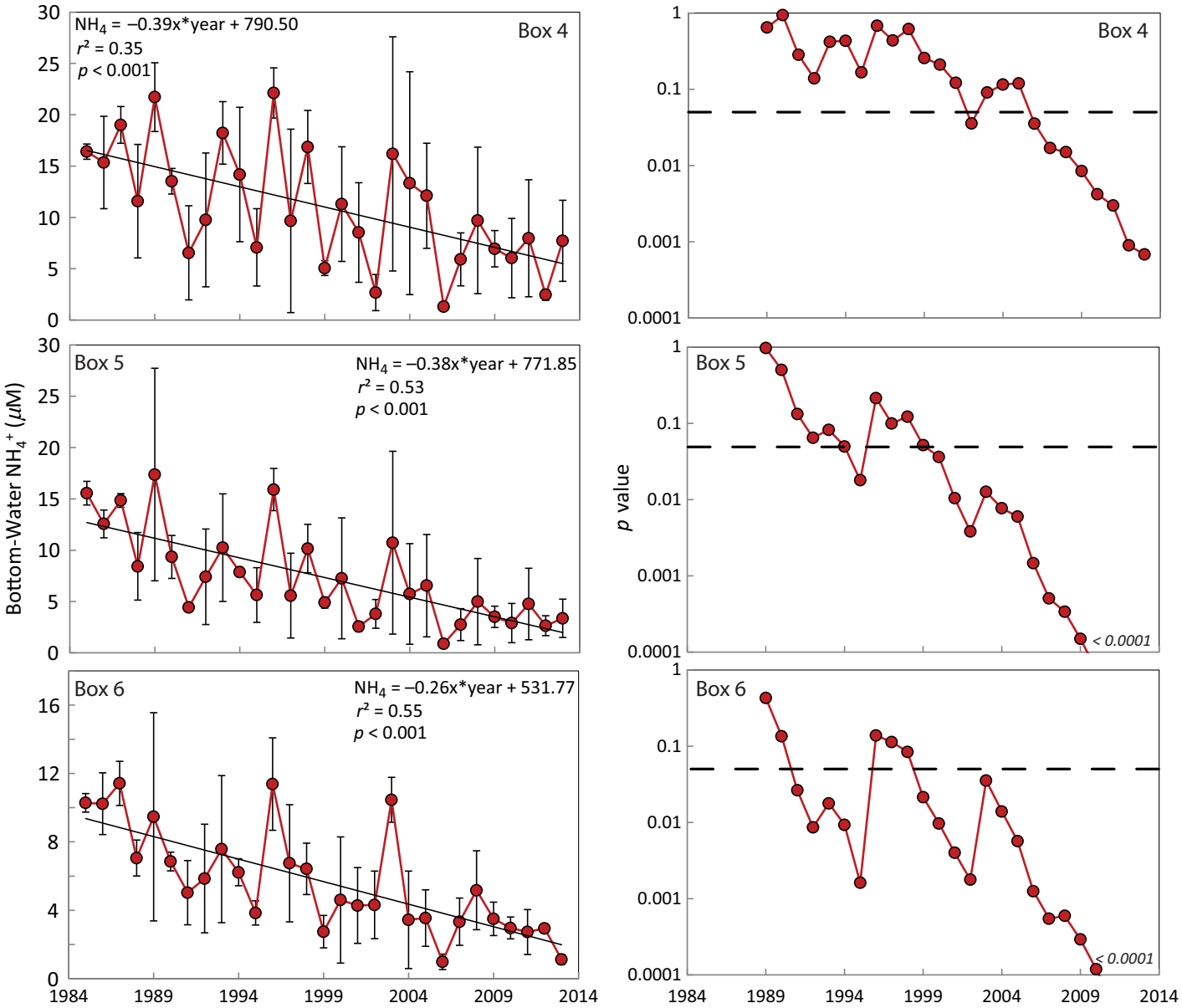

Fig. 3. Time series (1985–2013) of August to September bottom-layer NH_4^+ (left panels) in Boxes 4–6 (mid-Bay) (±SE) and associated *p* value for a simple linear regression of concentration and year (right panels) for all data prior to the given year (beginning in 1989, as the regression includes ≥ 5 yr of data). [Color figure can be viewed at wileyonlinelibrary.com]

Long-term trends in solute concentrations

While the seasonal variability in nitrogen forms in Chesapeake Bay is known to be substantial (Testa et al. 2018), interannual variability was also high (Figs. 3–5). This was especially true of bottom waters during the late-summer period (August to September), where concentrations of NH_4^+ decreased steadily during the two most recent decades, while oxygen and NO_{2+3}^- levels increased. Linear trends were significant ($p < 0.05$) for oxygen and dissolved nitrogen in the seasonally hypoxic region of the Bay (Figs. 3–5; Boxes 4–6, except NO_{2+3}^- in Box 4). The total decline in NH_4^+ from 1985 to 2013 was about 10 μM (~ 0.3 μM yr^{-1}), while the increase in NO_{2+3}^- approached 3–4 μM (0.15 μM yr^{-1}). Dissolved O_2 also increased to levels consistently above those considered to be severely hypoxic (62.5 μM) during this period.

Seasonal, regional, and decadal patterns in solute concentrations

NH_4^+ was depleted in surface waters and accumulated in bottom waters during the June to August period throughout the study region, resulting in strong vertical gradients (Fig. 6).

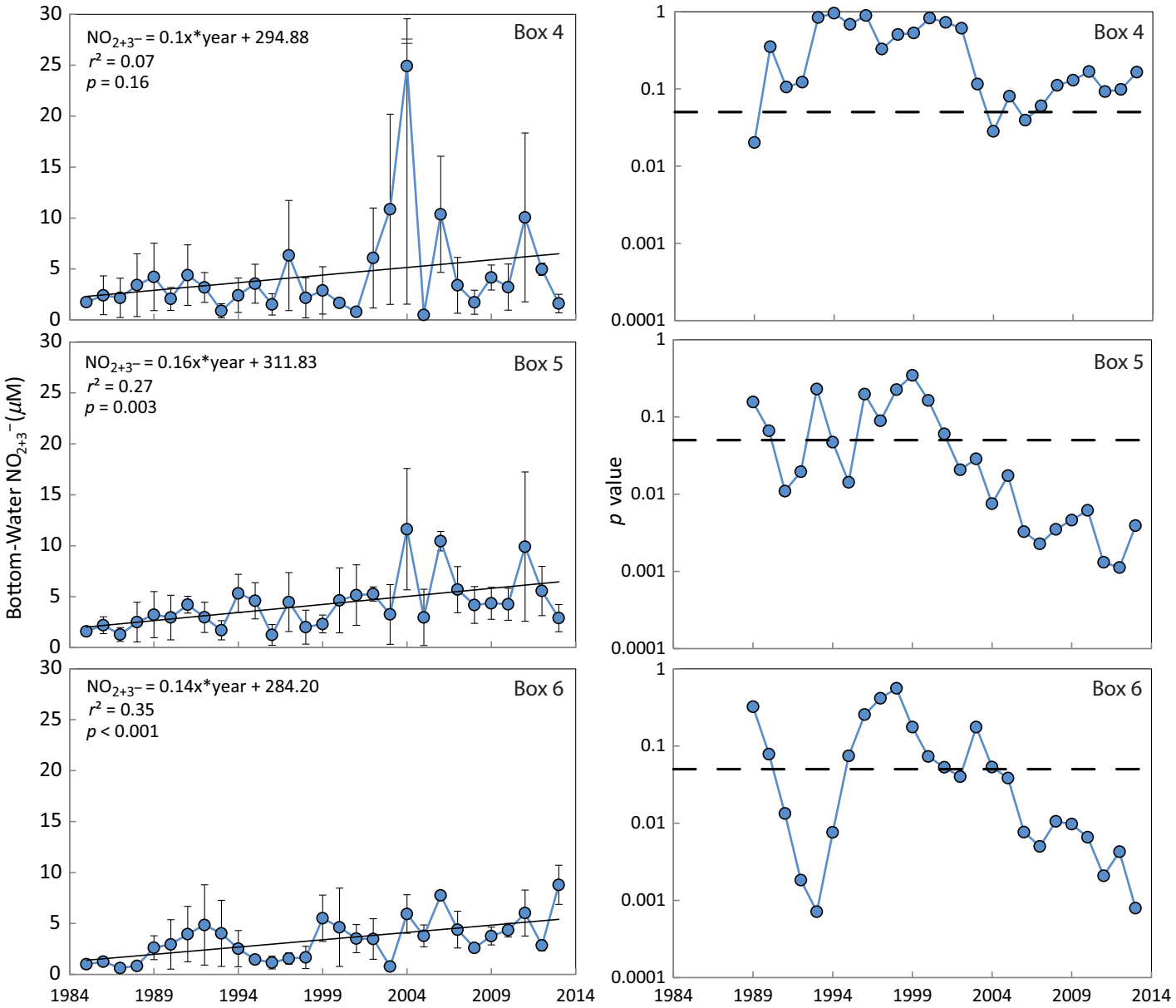

Fig. 4. Time series (1985–2013) of August to September bottom-layer NO_{2+3}^- (left panels) in Boxes 4–6 (mid-Bay) (± SE) and associated *p* value for a simple linear regression of concentration and year (right panels) for all data prior to the given year (beginning in 1989, as the regression includes ≥ 5 yr of data). [Color figure can be viewed at wileyonlinelibrary.com]

Average bottom water NH_4^+ concentrations ranged from 25 μM N in the northern region of the hypoxic zone (CB4.1C) with a large seaward gradient leading to minima of 10 μM N in the estuary's southern region (CB5.3). Dissolved NH_4^+ concentrations began to increase at 10 m in depth, consistent with the average location of the pycnocline. In general, bottom water concentrations were highest in the early-middle period (June to July) of the summer and begin to decline in August, where bottom water concentrations were consistently lower, especially at station CB4.4 and regions northward.

In contrast to NH_4^+, oxidized nitrogen forms (nitrate, NO_3^- and nitrite, NO_2^-) were uniformly low in the middle and deeper water-column during June and July, but increased rapidly to mean concentrations exceeding 5 μM in August and September (Fig. 6). This is especially true for NO_2^-, which increased to seasonal peaks in bottom water in late summer following extremely small concentrations in June and July. Bottom water NO_2^- concentrations were comparably high in the middle and lower region of the hypoxic zone (CB4.4 to CB5.3) and were often highest in

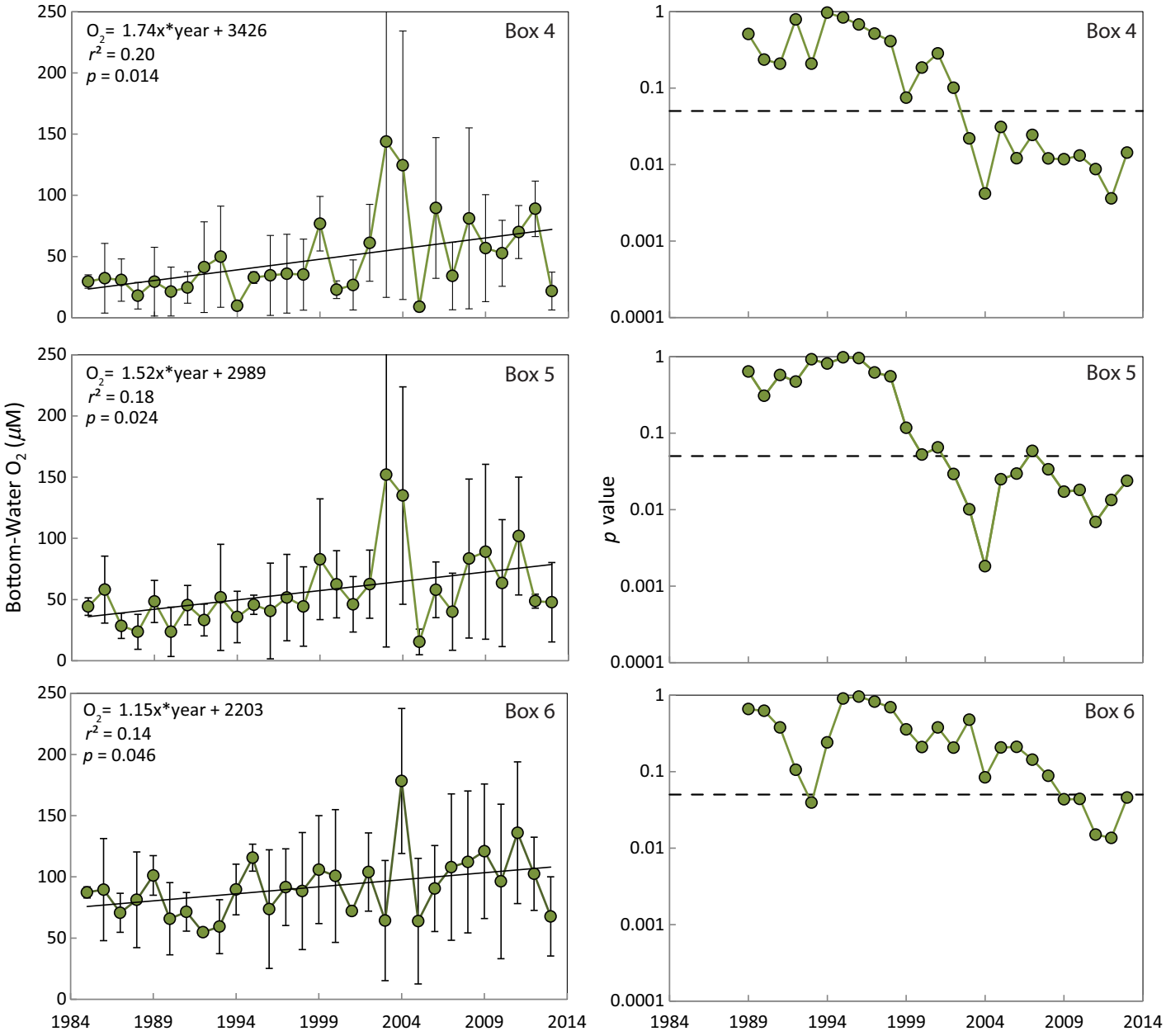

Fig. 5. Time series (1985–2013) of August to September bottom-layer dissolved O_2 (left panels) in Boxes 4–6 (mid-Bay) (± SE) and associated *p* value for a simple linear regression of concentration and year (right panels) for all data prior to the given year (beginning in 1989, as the regression includes ≥ 5 yr of data). [Color figure can be viewed at wileyonlinelibrary.com]

the middle of the water-column between 14 m and 22 m depth.

The long-term declines in later summer NH_4^+ and increases in NO_{2+3}^- were further examined by comparing vertical profiles in the first half of the time series (1985–1999) with the second half (2000–2014). The reduction in bottom water NH_4^+ concentration is clearly visible in waters below 10 m, despite high-interannual variability. The declines in NH_4^+ concentration were most visible in the middle and lower regions of the hypoxic zone (CB4.2C to CB5.3) where the long-term negative trends were most significant, but were not evident in surface waters or at stations in the oligohaline or polyhaline regions of Chesapeake Bay (data not shown). In contrast, increases in NO_2^- were only evident at stations CB5.1 to CB5.4, at the southern terminus of the seasonally hypoxic region. These changes represent a clear shift from NH_4^+ dominance in the 1985–1999 period to co-dominance with NO_2^- and NO_3^- in the 2000–2014 period.

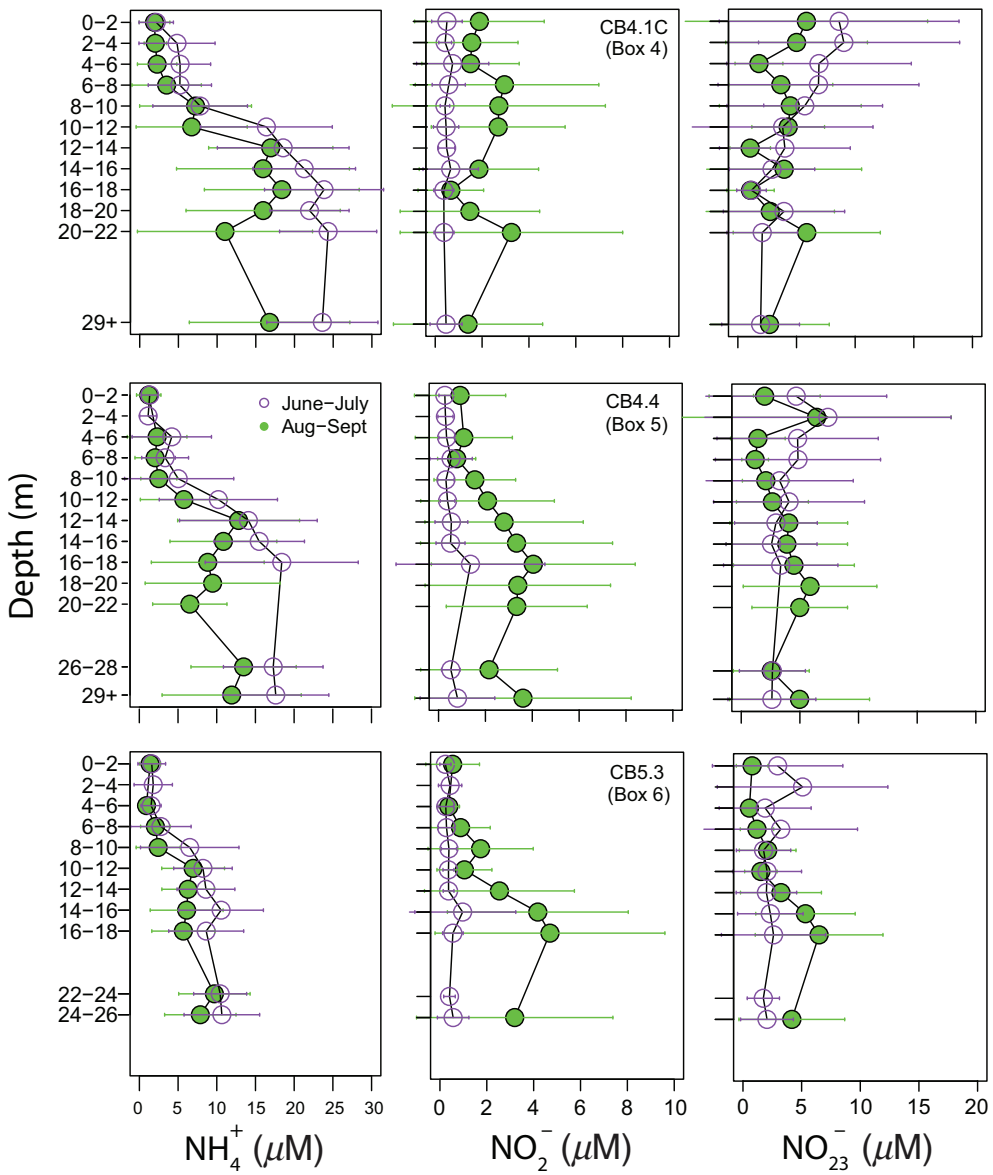

Fig. 6. Vertical profiles of ammonium (left), nitrite (middle), and nitrate (right) at three stations along the axis of Chesapeake Bay averaged over the 1985–2014 period for the months of June/July (purple circles) and August/September (green circles). CB4.1C is in Box 4, CB4.4 is in Box 5, and CB5.3 is in Box 6.

Net biogeochemical production and transport rates

Box-model-computed net nutrient and oxygen transformation rates provide estimates of the biogeochemical changes associated with altered nitrogen and oxygen concentrations. Annual cycles of the net production rates of NH_4^+, NO_{2+3}^-, NO_2^-, and O_2 in the bottom layer of Boxes 5 and 6 reveal changes in the magnitude of net transformation between 1985–1999 and 2000–2013. We chose this separation of periods because they represent an even split of the data into historic and recent periods and also because the relationship between Susquehanna River flow and nutrient load was significantly different during the two periods (ANCOVA; $F = 10.81$, $p = 0.0028$), suggesting a shift in the amount of nitrogen delivered by a given river flow. Net production rates of NH_4^+ declined sharply during August, September, and October during the last two decades (Fig. 7), corresponding to a sharp increase in the net production of NO_{2+3}^-. While net O_2 production rates were generally similar in these periods in Box 5, there was a slight increase in net oxygen uptake in Box 6 (Fig. 7). Wilcoxon Rank Sum tests were made to compare the differences between mean net production rates between the two periods (1985–1999 vs. 2000–2013; Fig. 7), and these tests indicated significant differences between the two groups ($p < 0.05$) for NO_{2+3}^- in July through October (Box 6) and

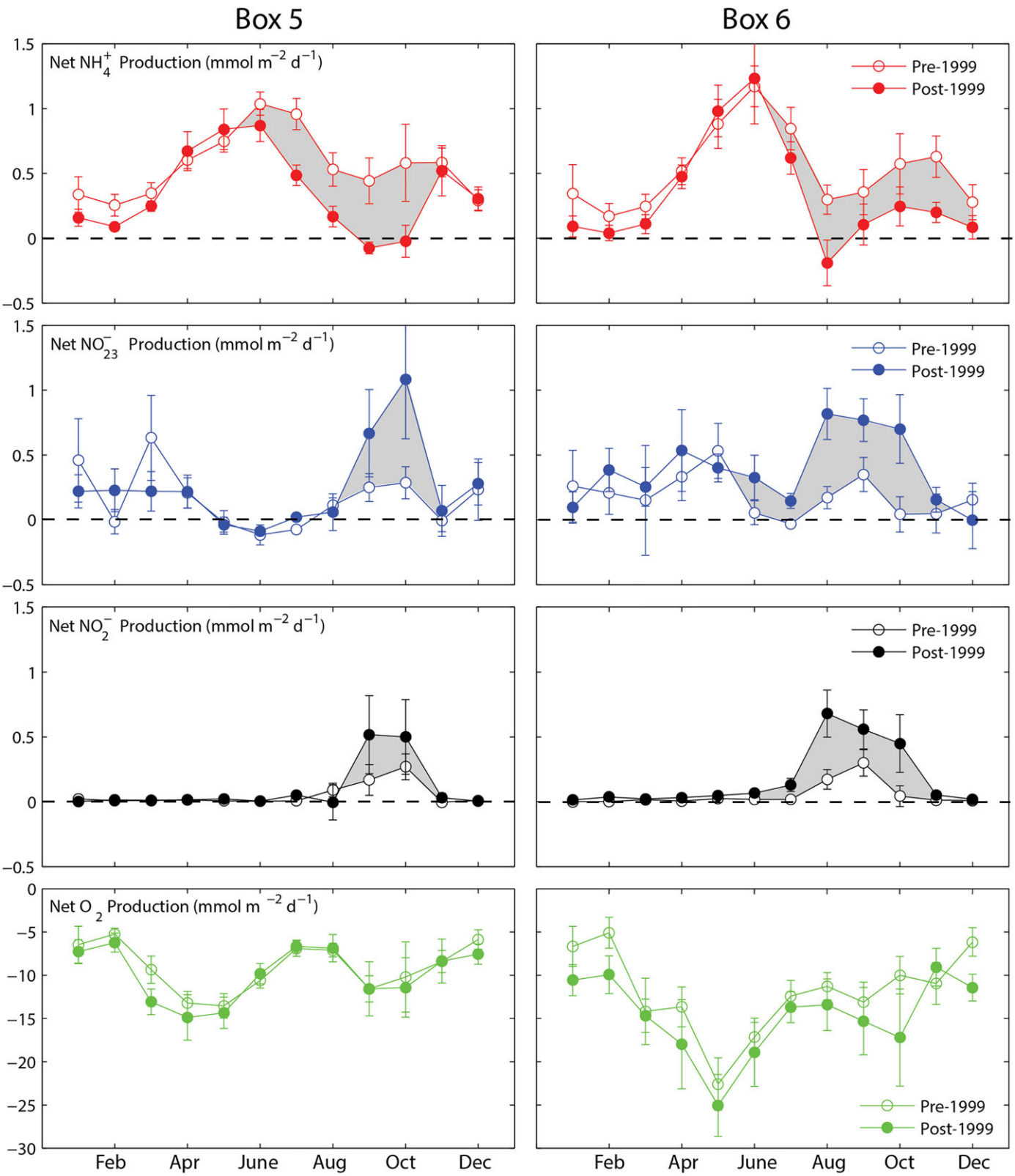

Fig. 7. Monthly mean net production rates of NH_4^+, NO_{2+3}^-, NO_2^-, and dissolved O_2 in the bottom layers of Box 5 (left panels), and Box 6 (right panels). Data are averaged for each month for the years 1985–1999 and 2000–2013.

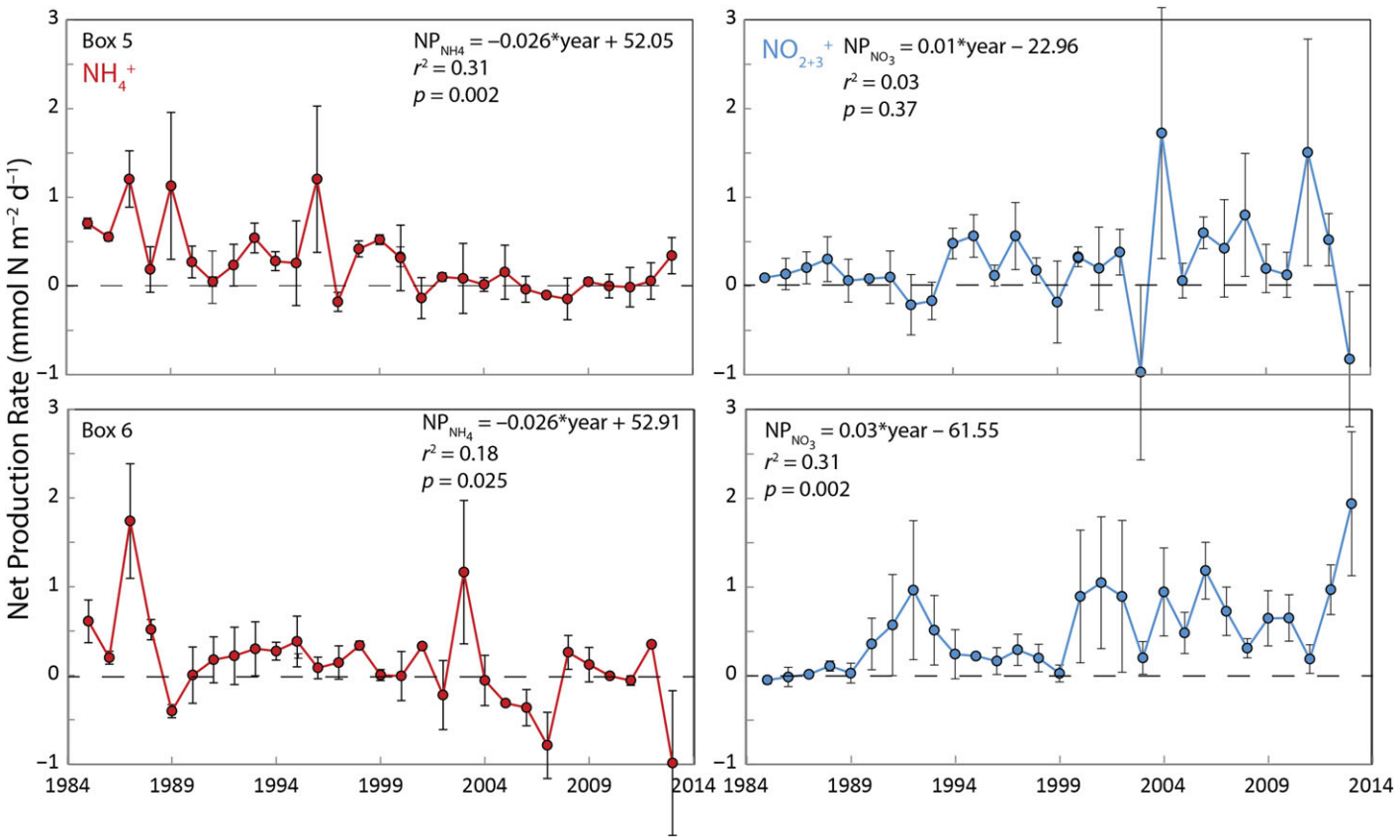

Fig. 8. Time series of August to September bottom-layer net NH_4^+ (left panels) and NO_{2+3}^- (right panels) production (NP) rates in two boxes (Boxes 5 and 6) within the middle Bay region from 1985 to 2013. Statistics (r^2, p value) for a simple linear regression of net production rate and year are included. [Color figure can be viewed at wileyonlinelibrary.com]

October (Box 5), for NH_4^+ in July to October (Box 5) and November (Box 6), and for NO_2^- in July, August, and October in Box 6. August and September differences in net NH_4^+ production in Box 6 were nearly significant ($p = 0.06$).

Times series of the bottom water production rates of NH_4^+ and NO_{2+3}^- in these two boxes further illustrates the long-term reduction in net NH_4^+ production (remineralization) and long-term increase in net NO_{2+3}^- production during the August to September period (Fig. 8). While slopes of linear regressions for net NO_{2+3}^- production were 0.01–0.03, slopes for net NH_4^+ production were ~ 0.027 for Boxes 5 and 6. Net Production of NO_{2+3}^- increased by 0.2–0.5 mmol N m^{-2} d^{-1} during the 30-yr period, while net NH_4^+ production decreased by 0.3–0.4 mmol N m^{-2} d^{-1}, which are comparable in magnitude.

In addition to the decline in net production of NH_4^+ in late summer, box-model computations indicated that landward advective transport of NH_4^+ into Box 6 (i.e., into the hypoxic zone) also declined in the late summer (Fig. 9). The reduction in advective NH_4^+ input over 1985–2013 was ~ 50% and corresponds to an increase of similar relative magnitude in the advective input of oxygen. The respective increases and decreases in advective, landward oxygen, and NH_4^+ flux in the late summer correspond to increases in oxygen concentration (and declines in NH_4^+ concentration) and not long-term changes in the magnitude of water flux. Thus, reductions in lower Bay concentrations of these solutes led to reductions in their landward transport. Similar long-term patterns were not evident in the early part of the summer and were muted for fluxes from more landward boxes.

Discussion

Dynamics of hypoxia in Chesapeake Bay

Intraseasonal changes in the extent of hypoxia in Chesapeake Bay have recently been documented (Murphy et al. 2011; Zhou et al. 2014). In general, the volume of hypoxic water has displayed a long-term increase during early summer (June and early July) and a long-term decline during late-July through September (i.e., late summer). Late-summer anoxic volumes have also contracted bay-wide in recent decades (Testa et al. 2017). While the exact mechanisms responsible for the late-summer oxygen increases are not fully understood at this time, our analysis reveals that the increases in bottom water oxygen are focused in the region of the Bay just north and south of the Potomac River (i.e., Box 7; Figs. 1 and 9). Similar patterns have been identified using other interpolation approaches (Zhou et al. 2014) and statistical models

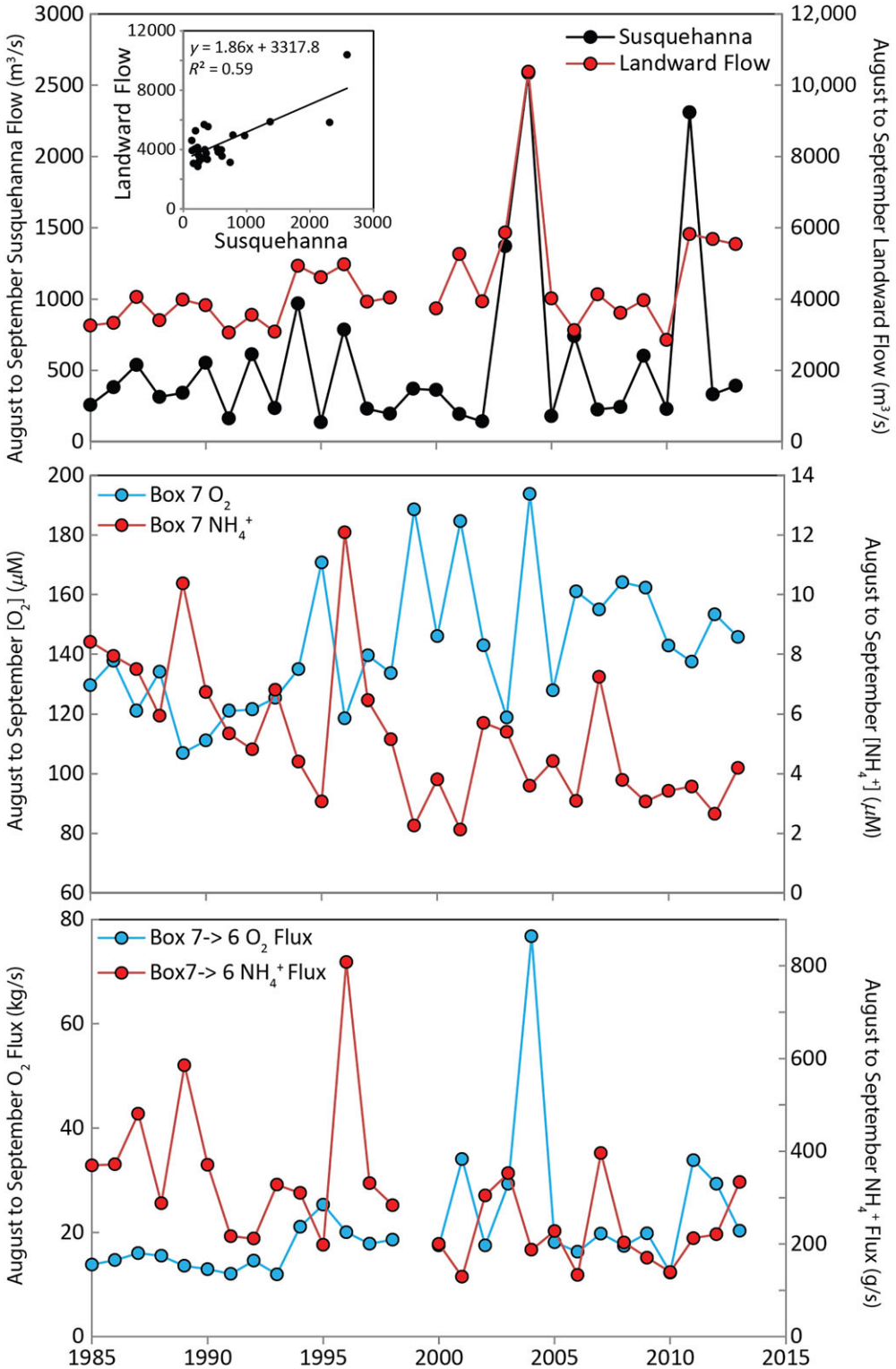

Fig. 9. Time series of mean August to September (top) Susquehanna River flow and advective flow into the bottom layer of Box 6, (middle) bottom-layer dissolved O_2 and NH_4^+ concentrations in Box 7, and (bottom) bottom-layer net landward transport from Box 7 to Box 6 of NH_4^+ and dissolved O_2. All computations and data are from the 1985–2013 period. Inset on top panel is correlation between Susquehanna River flow and advective flow into the bottom layer of Box 6.

of station-based, depth-specific oxygen concentration (e.g., generalized additive models; Testa et al. 2018). Hypoxic water in Chesapeake Bay initiates in landward bottom waters and expands southward over the course of summer (Testa and Kemp 2014) and the volume of hypoxia in waters south of the Potomac tends to expand during years of high-river flow and nutrient (nitrogen and phosphorus) inputs and contracts during years with low-river flow and/or low-nutrient inputs (Murphy et al. 2011).

Feedbacks between hypoxia and nitrogen cycling

Dissolved O_2 concentrations tend to control the cycling and availability of many key elements in marine environments (Glud 2008; Howarth et al. 2011), where low-dissolved O_2 levels can limit, e.g., coupled nitrification–denitrification and favor NH_4^+ recycling (Kemp et al. 1990). Testa and Kemp (2012) hypothesized that in the absence of oxygen, inhibition of nitrification leads to NH_4^+ accumulations that may feed back to support additional oxygen demand via the enhanced production of phytoplankton biomass supported by this increased supply of NH_4^+ in surface waters. This self-reinforcing, "positive feedback" appears to have been active in Chesapeake Bay during the early summer in recent decades, consistent with higher early summer hypoxic volumes (Murphy et al. 2011; Testa and Kemp 2012). Our findings in the present study, however, suggest an opposing "negative feedback" where even slightly elevated oxygen levels in late summer enabled elevated rates of nitrification, NH_4^+ removal, and presumably higher denitrification rates with NO_3^- diffusion into underlying sediments (Cornwell et al. 1999). This conclusion is supported by the increasing trends in late-summer bottom water dissolved O_2 and NO_{2+3}^- concentrations, increasing rates of net NO_{2+3}^- production (presumably net nitrification), and depressed net NH_4^+ production and availability. In addition, NH_4^+ concentrations in bottom water were positively correlated with watershed TN nutrient inputs over the 1985–2013 period, but the NH_4^+ concentration generated for a given TN input was lower in the 2000–2013 period than for 1985–1999, when bottom water oxygen concentrations were generally higher (Fig. 10). Such limits on NH_4^+ accumulation for a given nitrogen input may be associated with oxygenation and associated nitrification. Tight linkages between NH_4^+ availability and nitrification rate have been observed in many other systems worldwide (Soetaert et al. 2006; Sharp 2010).

Thus, the primary feature of this negative feedback is a shift toward an earlier breakup of hypoxic conditions and thus earlier enhancement of bottom water NH_4^+ oxidation, leading to reduced NH_4^+ concentrations and elevated bottom water NO_{2+3}^- concentrations. Given that TN inputs from the combined Susquehanna and Potomac Rivers to Chesapeake Bay have been recently declining (Zhang et al. 2015), there is no evidence to suggest that the NO_{2+3}^- concentration increases were due to changes in external load. The fact that NO_{2+3}^-

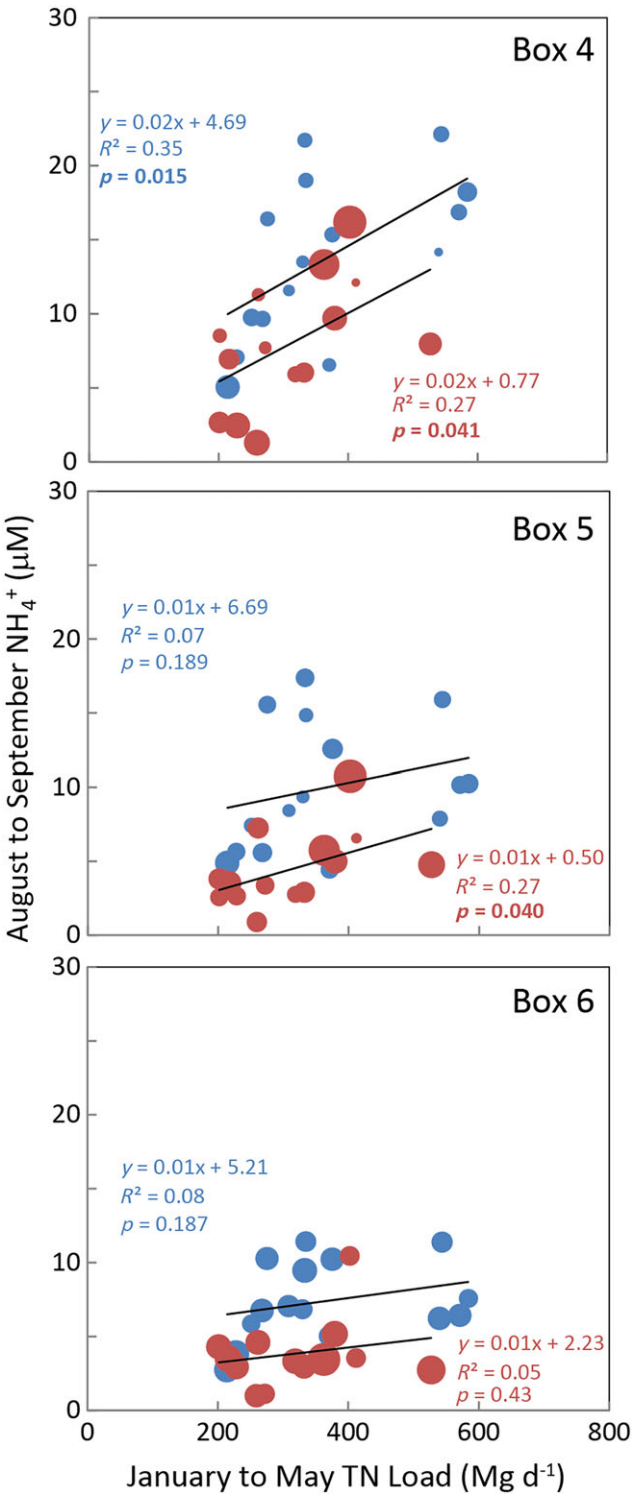

Fig. 10. Correlations between January to May TN loading to Chesapeake Bay from the Susquehanna and Potomac Rivers and August to September mean bottom water NH_4^+ concentrations, with data split between the 1985–1999 (blue circles) and 2000–2013 (red circles) period. Size of circles is scaled to August to September bottom water dissolved O_2 concentration. TN is the sum of all particulate and dissolved forms of organic and inorganic nitrogen, although primarily NO_{2+3}.

Table 2. Computations of oxygen consumption expected from box-model-computed net nitrification rates in three regions of Chesapeake Bay bottom waters (1985–2013 means). All rates in mmol O_2 m^{-3} d^{-1}. $\%O_2$ uptake is the percent of box-model-computed dissolved O_2 consumption attributed to net nitrification. NNN = no net nitrification computed.

	Box 4			Box 5			Box 6		
Month	NO_{2+3}^- NP	O_2 uptake	$\%O_2$ uptake	NO_{2+3}^- NP	O_2 uptake	$\%O_2$ uptake	NO_{2+3}^- NP	O_2 uptake	$\%O_2$ uptake
July	NNN	3.59	NNN	NNN	7.13	NNN	0.13	12.71	1.03
August	NNN	1.02	NNN	0.12	6.92	1.73	0.96	11.93	8.07
September	1.90	7.51	25.32	0.90	11.64	7.77	1.07	13.68	7.86
October	1.38	11.70	11.83	1.31	10.89	12.07	0.70	13.82	5.10

concentrations have only increased in sub-pycnocline waters during late-summer also suggests that internal production (i.e., nitrification) is the key mechanism driving the increase, as opposed to new watershed inputs that primarily impact surface waters during winter-spring. The late-summer (August to September) period is a time when hypoxic and anoxic conditions are usually diminished, as stratification weakens with declining water temperature and elevated wind speeds during the late summer and fall (Goodrich et al. 1987; Wilson et al. 2008) and vertical mixing of oxygen increases replenishment of bottom waters. In addition, the availability of labile organic matter tends to become limiting for respiration during late summer (Cowan and Boynton 1996, Boynton and Kemp 2008), and this contributes to reduced oxygen consumption rates. Thus, the negative-feedback is essentially enhancing the typical seasonal cycle that includes a late-summer recovery from hypoxic and anoxic conditons.

A key question related to the proposed negative feeback and associated NH_4^+ oxidation is the extent to which this nitrification could contribute to lags in oxygenation and hysteresis due to the fact that the process itself consumes oxygen. NH_4^+, like other reduced solutes (e.g., H_2S, CH_4), accumulates in hypoxic and anoxic basins (Zopfi et al. 2014; Gelesh et al. 2016) and serves as a potential reservoir of stored oxygen demand. Box-model calculated rates of net production of NH_4^+, NO_{2+3}^-, and oxygen for the hypoxic zone bottom layer in early and late summer provided quantitative estimates of these processes. Given that the box-model-derived rates provide estimates of net nonconservative behavior, they likely reflect conservative estimates of the gross rates. For example, a portion of the NO_{2+3}^- produced in a given month is denitrified, which would reduce the amount of NO_{2+3}^- accumulated from nitrification and underestimate the box-model-computed net NO_{2+3}^- production, thereby making the net production rate a conservative estimate of net nitrification (Kemp et al. 1990). A simple stoichiometric calculation of the expected oxygen consumption associated with the computed rates of net NO_{2+3}^- production (assuming O : N = 2, i.e., complete nitrification) indicates that nitrification consumed 1–2 mmol O_2 m^{-2} d^{-1}, which is generally < 10%; (Table 2) of box-model-computed O_2 consumption rates (which are actually estimates of the combined rate of sediment and water-column respiration). In fact, prior analyses suggest that the contribution of sediment nitrification to total sediment O_2 consumption fall within this range (Seitzinger et al. 1984; Henriksen and Kemp 1988).

While this additional O_2 consumption could explain some of the increased net oxygen consumption in bottom waters in lower regions of the Bay (Fig. 7), it is also possible that the elevation of dissolved O_2 availability (above hypoxic levels) in these waters during late summer relieved oxygen limitation of aerobic respiration (Sampou and Kemp 1994). Given that nitrification represents a net-zero change in available nitrogen, there is no reason to believe that these transformations would lead to different outcomes for new primary production and subsequent respiration if dissolved nitrogen is mixed into surface waters. Although net production rates from box-model calculations have inherent errors, these rates are comparable to measured rates of sediment-water fluxes and water-column transformation (e.g., McCarthy et al. 1984; Kemp et al. 1990; Cowan and Boynton 1996) and allow us to make tentative (but unprecidented), data-driven estimates of the relative contributions of respiration and nitrification to net ecosystem O_2 consumption in the hypoxic zone during early and late summer.

Relevance for nitrogen cycling

The nitrification rates we inferred for subsurface, mesohaline waters during late summer and early fall contrast with other previously identified nitrification "hotspots" in estuarine environments. Many previous studies have identified high-nitrification rates near low-salinity estuarine turbidity maxima (Iriarte et al. 1996; Brion et al. 2000; Damashek et al. 2016) and have associted these high rates with particle-dominated microbial communities, and with NH_4^+ sorption and desorption, as well as elevated heterotrophic activity. Low-salinity regions of estuaries have also been locations where extremely high-wastewater discharges of NH_4^+ have supported high-nitrification rates (Lipschultz et al. 1986; Gazeau 2005; Soetaert et al. 2006; Aissa-Grouz et al. 2015) and contributed to oxygen depletion. While the nitrification bursts that occur during vertical mixing in seasonally stratified and

hypoxic systems may be short lived (Horrigan et al. 1990), they potentially contribute substantially to annual cycles of inorganic nitriogen species and can support denitrification in underlying sediments during this period (Kemp et al. 1990).

Given the emphasis on nitrification in the present analysis, it is clear that nitrite (NO_2^-) cycling is a previously recognized, but generally unquantified and underappreciated process involved in estuarine nitrogen dynamics. NO_2^- accumulation in aerobic coastal marine waters has been associated with both NH_4^+ oxidation and assimilatory NO_3^- reduction (Zehr and Ward 2002) and nitrite peaks have commonly been observed in a wide range of coastal environments, including the base of the euphotic zones and in oxygen-poor regions (Beman et al. 2013; Santoro et al. 2013). Prior studies have identified clear and substantial peaks (4–10 μM) in NO_2^- concentration during fall turnover in Chesapeake Bay (McCarthy et al. 1977) driven by the oxidation of accumulated NH_4^+ pools in bottom water underlying the pycnocline. It was unclear if these presumably large rates of nitrification were too short lived to affect nitrogen cycling overall and whether they would become more substantial or prolonged under more extensive anoxia (McCarthy et al. 1984). The appearance of elevated NO_2^- in Chesapeake Bay bottom waters is spatially and temporally linked to accumulated bottom water NH_4^+ and indicates nitrification for several reasons. First, corresponding increases in NO_{2+3}^- concentrations (of which NO_2^- is a component) have increased in the late summer at a rate comparable to the NH_4^+ decline (Figs. 3–4). Second, reductions in box-model-computed rates of net NH_4^+ production were quantitatively similar to increases in net NO_{2+3}^- production (Fig. 7). Finally, box-model-derived estimates of net NO_{2+3}^- production (208 ± 91 nmol l^{-1} d^{-1} annual mean ± SE and 352 ± 101 nmol l^{-1} d^{-1} August to September mean ± SE) rates fall well within the range of previously reported direct measurements of nitrification rates in this region of Chesapeake Bay (McCarthy et al. 1984; Horrigan et al. 1990). Mean box-model rates are slightly lower than reported nitrification rates, which is consistent with the fact that sediments typically consume NO_{2+3}^- (e.g., denitrification) during this period at rates that peak at 50–75 nmol l^{-1} d^{-1} (Cowan and Boynton 1996), which would have the effect of lowering the net production rate. Both box-model computations in Chesapeake Bay and observations in this and other eutrophic estuaries (e.g., Horrigan et al. 1990; Berounsky and Nixon 1993; Damashek et al. 2016) have indicated pulses of extremely high-nitrification rates (> 5000 nmol l^{-1} d^{-1}), which underscores the variability in this process. Clearly, new and expanded measurements of nitrification during this late-summer period are needed using a suite of modern techniques to help clarify the mechanisms and magnitudes of key nitrogen cycling processes.

Summary and synthesis

We have summarized our current understanding of these coupled processes of nitrogen and oxygen cycling in a conceptual model (Fig. 11) that contrasts the earlier and later periods of the warmer seasons of the year. In spring, high rates of nitrogen inputs, which are dominated by NO_3^-, support high rates of phytoplankton production and associated particulate organic nitrogen sinking (Hagy et al. 2005) that convert the dissolved nitrogen pool into particulate nitrogen (PN) forms (Fig. 11). Strong stratification that is forced by high-river flow during this season limits reoxygenation of bottom water and generally allows NH_4^+ to accumulate in deeper waters, as nitrification is inhibited by low-dissolved O_2 (Kemp et al. 1990; Murphy et al. 2011; Testa and Kemp 2012). Similar patterns of bottom water NH_4^+ accumulation under stratified conditions have been reported in other estuarine and coastal systems (Zopfi et al. 2014; Kuypers et al. 2003). In contrast, late summer and fall are characterized by seasonal minima in watershed nitrogen loading and relatively low phytoplankton biomass (Fig. 11; e.g., Roman et al. 2005) and organic matter deposition to sediments (except following large storms; Miller et al. 2006). Stratification is reduced in late summer and fall by severe storms and/or surface cooling, which promote reoxygenation of the bottom waters as well as enhanced nitrification rates and NO_2^- and NO_3^- concentrations (Fig. 11). All of these processes limit the accumulation of NH_4^+ during this season.

The long-term changes we observed in Chesapeake Bay are an important modulation of this seasonal cycle. Recent analyses have shown that reduced Susquehanna River nitrogen loads have been associated with a reduction of the spring bloom in lower Bay regions (Testa et al. 2018). As a consequence, less PN would have been available to support NH_4^+ remineralization fluxes in bottom waters (Cowan and Boynton 1996) and associated oxygen depletion as the summer progressed (Testa et al. 2017). In recent decades, late-summer and fall dissolved O_2 concentrations thus increased earlier and faster than they probably did during summer-fall turnover events in earlier decades, allowing for higher nitrification rates that would enhance NO_{2+3}^- availability to support higher rates of denitrification (Kemp et al. 1990). Our analyses suggest that a series of coupled reactions over the course of the warm season explained the observed data patterns. It is clear, however, that further observational, experimental, and diagnostic modeling studies are needed to test the hypothesis that reoxygenation-induced nitrification can be a significant process for stratified estuarine ecosystems recovering from eutrophication. Regardless of the long-term drivers of such changes, the linked alterations of the carbon, oxygen, and nitrogen cycles represented here demand continued study.

Implications for eutrophication science

The documentation of long-term changes in the cycling of dissolved nitrogen associated with changes in oxygen availability highlights several previously underappreciated aspects of estuarine response to reductions in eutrophication. First, changes in nitrogen cycling associated with oxygen availability will alter the forms of dissolved nitrogen occuring in the estuary (e.g., NO_{2+3}^- vs. NH_4^+) in response to changing nutrient inputs and resulting changes in nitrification rates. While

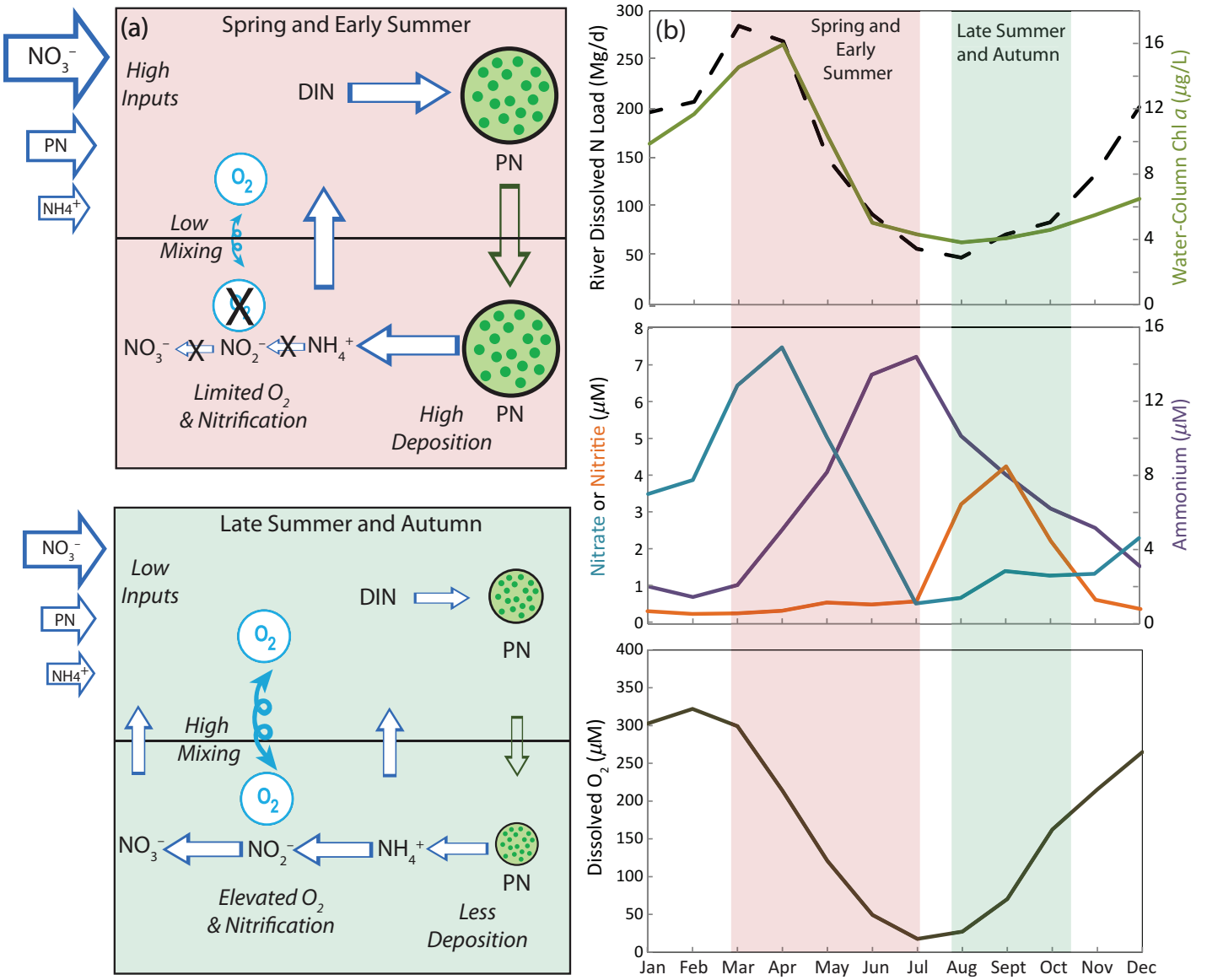

Fig. 11. (**a**) Conceptual diagram of nitrogen transport and cycling in spring and early summer months vs. late-summer and autumn months. Spring and early summer are characterized by elevated nitrogen loads, a spring phytoplankton bloom, and eventual oxygen depletion and NH_4^+ accumulation associated with high stratification and PN deposition. Late summer and autumn include lower phytoplankton production and elevated vertical mixing, which serve to replenish dissolved O_2 and support nitrification. (**b**) Mean seasonal cycles of Susquehanna River total dissolved nitrogen loads, water-column chl *a* (integrated over all depths), and bottom water inorganic N and dissolved O_2 are included for a mid-Bay station (1985–2015 mean values) to support the seasonal patterns described by the conceptual diagram.

many aspects of the linkages between oxygen availability and nitrogen cycling have been investigated elsewhere, our analysis is unique in that it describes how long-term changes in the availability of oxygen caused large changes in the rates of nitrogen transformation over expansive regions of a eutrophic estuary and we are aware of no similar reports from other seasonally stratified estuaries. Second, while annually averaged metrics of constituent concentrations are often used to track eutrophication status, intraseasonal changes in key constituents and season-specific trends (e.g., spring, late summer) may reveal fundamental mechanisms and trajectories associated with ecosystem responses to changes in nutrient inputs. For example, we might expect recovery from eutrophication to manifest first during the late growing season in seaward estuarine reaches, where nutrient limitation would be first realized (Fisher et al. 1992; Riemann et al. 2016). Finally, it is clear from this analysis that water quality monitoring programs maintained for decades with full seasonal coverage can reveal complex dynamics in systems undergoing recovery from eutrophication (Tucker et al. 2014; Stæhr et al. 2017). In our analyses for Chesapeake Bay, significant trends in NO_{2+3}^-, NH_4^+, and oxygen concentration did not emerge until a decade after the first

signs of responses to nutrient input reduction were evident in 1990 (Zhang et al. 2015), but if we had known where to look for these trends, they would have been available for discovery at least 10 yr before the present (Figs. 3–5). Clearly, responses to eutrophication abatement may be gradual and involve lags, which underscores the need for sustained monitoring investments. Data generated by these programs can be used to address compelling scientific questions, many of which are relevant for adressing pressing management challenges.

References

Aissa-Grouz, N., J. Garnier, G. Billen, B. Mercier, and A. Martinez. 2015. The response of river nitrification to changes in wastewater treatment (the case of the lower Seine River downstream from Paris). Ann. Limnol. Int. J. Lim. **51**: 351–364. doi:10.1051/limn/2015031

Andersen, J. H., and others. 2015. Long-term temporal and spatial trends in eutrophication status of the Baltic Sea. Biol. Rev. **39**: 664–681. doi:10.1111/brv.12221

Beman, J. M., J. L. Shih, and B. N. Popp. 2013. Nitrite oxidation in the upper water column and oxygen minimum zone of the eastern tropical North Pacific Ocean. ISME J. **7**: 2192. doi:10.1038/ismej.2013.96

Berounsky, V. M., and S. W. Nixon. 1993. Rates of nitrification along an estuarine gradient in Narragansett Bay. Estuaries **16**: 718–730. doi:10.2307/1352430

Boynton, W. R., J. H. Garber, R. Summers, and W. M. Kemp. 1995. Inputs, transformations, and transport of nitrogen and phosphorus in Chesapeake Bay and selected tributaries. Estuaries **18**: 285–314. doi:10.2307/1352640

Boynton, W. R., and W. M. Kemp. 2008. Estuaries. p. 809–866. *In* D. G. Capone, D. A. Bronk, M. R. Mulholland and E. J. Carpenter [eds.], Nitrogen in the marine environment. Amsterdam: Elsevier.

Boynton, W. R., and others. 2008. Nutrient budgets and management actions in the Patuxent River estuary, Maryland. Estuar. Coast. **31**: 623–651. doi:10.1007/s12237-008-9052-9

Boynton, W. R., C. L. S. Hodgkins, C. A. O'Leary, E. M. Bailey, A. R. Bayard, and L. A. Wainger. 2014. Multi-decade responses of a tidal creek system to nutrient load reductions: Mattawoman Creek, Maryland USA. Estuar. Coast. **37**: 111–127. doi:10.1007/s12237-013-9690-4

Brion, N., G. Billen, L. Guézennec, A. Ficht, L. Guezennec, and A. Ficht. 2000. Distribution of nitrifying activity in the Seine River (France) from Paris to the estuary. Estuaries **23**: 669–682. doi:10.2307/1352893

Cloern, J. E. 2001. Our evolving conceptual model of the coastal eutrophication problem. Mar. Ecol. Prog. Ser. **210**: 223–253. doi:10.3354/meps210223

Cloern, J. E., and A. D. Jassby. 2010. Patterns and scales of phytoplankton variability in estuarine and coastal ecosystems. Estuar. Coast. **33**: 230–241. doi:10.1007/s12237-009-9195-3

Conley, D. J., C. Humborg, L. Rahm, O. P. Savchuk, and F. Wulff. 2002. Hypoxia in the Baltic Sea and basin-scale changes in phosphorus biogeochemistry. Environ. Sci. Technol. **36**: 5315–5320. doi:10.1021/es025763w

Cornwell, J. C., and P. A. Sampou. 1995. Environmental controls on iron sulfide mineral formation in a coastal plain estuary, p. 224–242. *In* M. A. Vairamurthy and M. A. A. Schoonen [eds.], Geochemical transformations of sedimentary sulfur. American Chemical Society.

Cornwell, J. C., W. M. Kemp, and T. M. Kana. 1999. Denitrification in coastal ecosystems: Environmental controls and aspects of spatial and temporal scaling. Aquat. Ecol. **33**: 41–54. doi:10.1023/A:1009921414151

Cowan, J. L., and W. R. Boynton. 1996. Sediment-water oxygen and nutrient exchanges along the longitudinal axis of Chesapeake Bay: Seasonal patterns, controlling factors and ecological significance. Estuaries **19**: 562–580. doi:10.2307/1352518

Cronin, W. B., and D. W. Pritchard. 1975. Additional statistics on the dimensions of Chesapeake Bay and its tributaries: Cross-section widths and segment volumes per meter depth, p. 475. Chesapeake Bay Institute, The Johns Hopkins Univ.

Damashek, J., K. L. Casciotti, and C. A. Francis. 2016. Variable nitrification rates across environmental gradients in turbid, nutrient-rich estuary waters of San Francisco Bay. Estuar. Coast. **39**: 1050–1071. doi:10.1007/s12237-016-0071-7

Díaz, R. J., and R. Rosenberg. 2008. Spreading dead zones and consequences for marine ecosystems. Science **321**: 926–929. doi:10.1126/science.1156401

Duarte, C. M., D. J. Conley, J. Carstensen, and M. Sánchez-Camacho. 2009. Return to Neverland: shifting baselines affect eutrophication restoration targets. Estuar. Coast. **32**: 29–36. doi:10.1007/s12237-008-9111-2

Fisher, T. R., E. R. Peele, J. W. Ammerman, and J. L. W. Harding. 1992. Nutrient limitation of phytoplankton in Chesapeake Bay. Mar. Ecol. Prog. Ser. **82**: 51–63. doi:10.3354/meps082051

Gazeau, F., J.-P. Gattuso, J. J. Middelburg, N. Brion, L.-S. Schiettecatte, M. Frankignoulle, and A. V. Borges. 2005. Planktonic and whole system metabolism in a nutrient-rich estuary (the Scheldt estuary). Estuar. Coast. **28**: 868–883. doi:10.1007/BF02696016

Gelesh, L., K. Marshall, W. C. Boicourt, and L. Lapham. 2016. Methane concentrations increase in bottom waters during summertime anoxia in the highly eutrophic estuary, Chesapeake Bay, U.S.A. Limnol. Oceanogr. **61**: S253–S266. doi:10.1002/lno.10272

Glud, R. N. 2008. Oxygen dynamics of marine sediments. Mar. Biol. Res. **4**: 243–289. doi:10.1080/17451000801888726

Goodrich, D. M., W. C. Boicourt, P. Hamilton, and D. W. Pritchard. 1987. Wind-induced destratification in Chesapeake Bay. J. Phys. Oceanogr. **17**: 2232–2240. doi:10.1175/1520-0485(1987)017<2232:WIDICB>2.0.CO;2

Greening, H., and A. Janicki. 2006. Toward reversal of eutrophic conditions in a subtropical estuary: Water quality and seagrass response to nitrogen loading reductions in Tampa Bay, Florida, USA. Environ. Manage. **38**: 163–178. doi:10.1007/s00267-005-0079-4

Gurbisz, C., and W. M. Kemp. 2014. Unexpected resurgence of a large submersed plant bed in Chesapeake Bay: Analysis of time series data. Limnol. Oceanogr. **59**: 482–494. doi:10.4319/lo.2014.59.2.0482

Hagy, J. D., L. P. Sanford, and W. R. Boynton. 2000. Estimation of net physical transport and hydraulic residence times for a coastal plain estuary using box models. Estuaries **23**: 328–340. doi:10.2307/1353325

Hagy, J. D. 2002. Eutrophication, hypoxia, and trophic transfer efficiency in Chesapeake Bay. Ph.D., University of Maryland, College Park College Park, Maryland.

Hagy, J. D., W. R. Boynton, C. W. Keefe, and K. V. Wood. 2004. Hypoxia in Chesapeake Bay, 1950–2001: Long-term change in relation to nutrient loading and river flow. Estuaries **27**: 634–658. doi:10.1007/BF02907650

Hagy, J. D., W. R. Boynton, and D. A. Jasinski. 2005. Modeling phytoplankton deposition to Chesapeake Bay sediments during winter-spring: Interannual variability in relation to river flow. Estuar. Coast. Shelf Sci. **62**: 25–40. doi:10.1016/j.ecss.2004.08.004

Harding, L. W., and E. Perry. 1997. Long-term increase of phytoplankton biomass in Chesapeake Bay, 1950–1994. Mar. Ecol. Prog. Ser. **157**: 39–52. doi:10.3354/meps157039

Harding, L. W., and others. 2015*a*. Climate effects on phytoplankton floral composition in Chesapeake Bay. Estuar. Coast. Shelf Sci. **162**: 53–68. doi:10.1016/j.ecss.2014.12.030

Harding, L. W., and others. 2015*b*. Long-term trends of nutrients and phytoplankton in Chesapeake Bay. Estuar. Coast. **39**: 664–681. doi:10.1007/s12237-015-0023-7

Henriksen, K., and W. M. Kemp. 1988. Nitrification in estuarine and coastal marine sediments, p. 207–249. *In* T. H. Blackburn and J. Sørensen [eds.], Nitrogen cycling in coastal marine environments. John Wiley & Sons.

Horrigan, S. G., and others. 1990. Nitrogenous nutrient transformations in the spring and fall in the Chesapeake Bay. Estuar. Coast. Shelf Sci. **30**: 369–391. doi:10.1016/0272-7714(90)90004-B

Howarth, R. W., and R. Marino. 2006. Nitrogen as the limiting nutrient for eutrophication in coastal marine ecosystems: Evolving views over three decades. Limnol. Oceanogr. **51**: 364–376. doi:10.4319/lo.2006.51.1_part_2.0364

Howarth, R., and others. 2011. Coupled biogeochemical cycles: Eutrophication and hypoxia in temperate estuaries and coastal marine ecosystems. Front. Ecol. Environ. **9**: 18–26. doi:10.1890/100008

Iriarte, A., I. D. Madariaga, F. Diez-Garagarza, M. Revilla, and E. Orive. 1997. Primary plankton production, respiration and nitrification in a shallow temperate estuary during summer. J. Exp. Mar. Biol. Ecol. **208**: 127–151. doi:10.1016/S0022-0981(96)02672-X

Joye, S. B., and J. T. Hollibaugh. 1995. Influence of sulfide inhibition of nitrification on nitrogen regeneration in sediments. Science **270**: 623–625. doi:10.1126/science.270.5236.623

Kemp, W. M., P. Sampou, J. Caffrey, M. Mayer, K. Henriksen, and W. R. Boynton. 1990. Ammonium recycling versus denitrification in Chesapeake Bay sediments. Limnol. Oceanogr. **35**: 1545–1563. doi:10.4319/lo.1990.35.7.1545

Kemp, W. M., and others. 2005. Eutrophication of Chesapeake Bay: Historical trends and ecological interactions. Mar. Ecol. Prog. Ser. **303**: 1–29. doi:10.3354/meps303001

Kemp, W. M., J. M. Testa, D. J. Conley, D. Gilbert, and J. D. Hagy. 2009. Temporal responses of coastal hypoxia to nutrient loading and physical controls. Biogeosciences **6**: 2985–3008. doi:10.5194/bg-6-2985-2009

Kuypers, M. M. M., and others. 2003. Anaerobic ammonium oxidation by anammox bacteria in the Black Sea. Nature **422**: 608–611. doi:10.1038/nature01472

Lipschultz, F., S. C. Wofsy, and L. E. Fox. 1986. Nitrogen metabolism of the eutrophic Delaware River ecosystem. Limnol. Oceanogr. **31**: 701–716. doi:10.4319/lo.1986.31.4.0701

McCarthy, J. J., W. R. Taylor, and J. L. Taft. 1977. Nitrogenous nutrition of the plankton in the Chesapeake Bay. I. Nutrient availability and phytoplankton preferences. Limnol. Oceanogr. **22**: 996–1011. doi:10.4319/lo.1977.22.6.0996

McCarthy, J. J., W. Kaplan, and J. L. Nevins. 1984. Chesapeake Bay nutrient and plankton dynamics. 2. Sources and sinks of nitrite. Limnol. Oceanogr. **29**: 84–98. doi:10.4319/lo.1984.29.1.0084

Miller, W. D., L. W. Harding, and J. E. Adolf. 2006. Hurricane Isabel generated an unusual fall bloom in Chesapeake Bay. Geophys. Res. Lett. **33**: L06612. doi:10.1029/2005GL025658

Murphy, R. R., W. M. Kemp, and W. P. Ball. 2011. Long-term trends in Chesapeake Bay seasonal hypoxia, stratification, and nutrient loading. Estuar. Coast. **34**: 1293–1309. doi:10.1007/s12237-011-9413-7

Newcombe, C. L., and W. A. Horne. 1938. Oxygen-poor waters of the Chesapeake Bay. Science **88**: 80–81. doi:10.1126/science.88.2273.80

Nixon, S. W. 1995. Coastal marine eutrophication: A definition, social causes, and future concerns. Ophelia **41**: 199–219. doi:10.1080/00785236.1995.10422044

Officer, C. B. 1980. Box models revisited, p. 65–114. *In* P. Hamilton and R. B. Macdonald [eds.], Estuarine and wetland processes. Plenum Press.

Orth, R., and others. 2010. Long-term trends in submersed aquatic vegetation (SAV) in Chesapeake Bay, USA, related to water quality. Estuar. Coast. **33**: 1144–1163. doi:10.1007/s12237-010-9311-4

Paerl, H. W., L. M. Valdes, B. L. Peierls, J. E. Adolf, and J. L. W. Harding. 2006. Anthropogenic and climatic influences on the eutrophication of large estuarine systems. Limnol. Oceanogr. **51**: 448–462. doi:10.4319/lo.2006.51.1_part_2.0448

Pritchard, D. W. 1969. Dispersion and flushing of pollutants in estuaries. Am. Soc. Civil Eng. J. Hydraul. Div. **95**: 115–124.

Rabalais, N. N., and others. 2014. Eutrophication-driven deoxygenation in the coastal ocean. Oceanography **27**: 172–183. doi:10.5670/oceanog.2014.21

Riemann, B., and others. 2016. Recovery of Danish coastal ecosystems after reductions in nutrient loading: A holistic ecosystem approach. Estuar. Coast. **39**: 82–97. doi:10.1007/s12237-015-9980-0

Roman, M., X. Zhang, C. McGilliard, and W. Boicourt. 2005. Seasonal and annual variability in the spatial patterns of plankton biomass in Chesapeake Bay. Limnol. Oceanogr. **50**: 480–492. doi:10.4319/lo.2005.50.2.0480

Sale, J. W., and W. W. Skinner. 1917. The vertical distribution of dissolved oxygen and the precipitation by salt water in certain tidal areas. J. Franklin Inst. **184**: 837–848. doi:10.1016/S0016-0032(17)90519-8

Sampou, P., and W. M. Kemp. 1994. Factors regulating plankton community respiration in Chesapeake Bay. Mar. Ecol. Prog. Ser. **110**: 249–258. doi:10.3354/meps110249

Santoro, A. E., and others. 2013. Measurements of nitrite production in and around the primary nitrite maximum in the central California Current. Biogeosciences **10**: 5803. doi:10.5194/bgd-10-5803-2013

Scully, M. E. 2010. Wind modulation of dissolved oxygen in Chesapeake Bay. Estuar. Coast. **33**: 1164–1175. doi:10.1007/s12237-010-9319-9

Seitzinger, S. P., S. W. Nixon, and M. E. Q. Pilson. 1984. Denitrification and nitrous oxide production in a coastal marine ecosystem1. Limnol. Oceanogr. **29**: 73–83. doi:10.4319/lo.1984.29.1.0073

Sharp, J. H. 2010. Estuarine oxygen dynamics: what can we learn about hypoxia from long-time records in the Delaware estuary? Limnol. Oceanogr. **55**: 535–548.

Soetaert, K., J. J. Middelburg, C. Heip, P. Meire, S. V. Damme, and T. Maris. 2006. Long-term change in dissolved inorganic nutrients in the heterotrophic Scheldt estuary (Belgium, The Netherlands). Limnol. Oceanogr. **51**: 409–423. doi:10.4319/lo.2006.51.1_part_2.0409

Staehr, P. A., J. Testa, and J. Carstensen. 2017. Decadal changes in water quality and net productivity of a shallow Danish estuary following significant nutrient reductions. Estuar. Coast. **40**: 63–79. doi:10.1007/s12237-016-0117-x

Testa, J. M., and W. M. Kemp. 2012. Hypoxia-induced shifts in nitrogen and phosphorus cycling in Chesapeake Bay. Limnol. Oceanogr. **57**: 835–850. doi:10.4319/lo.2012.57.3.0835

Testa, J. M., and W. M. Kemp. 2014. Spatial and temporal patterns in winter-spring oxygen depletion in Chesapeake Bay bottom waters. Estuar. Coast. **37**: 1432–1448. doi:10.1007/s12237-014-9775-8

Testa, J. M., and others. 2017. Modeling physical and biogeochemical controls on dissolved oxygen in Chesapeake Bay: Lessons learned from simple and complex approaches. *In* D. Justic, K. Rose, R. Hetland, and K. Fennel [eds.], Modeling coastal hypoxia—Numerical simulations of patterns, controls and effects of dissolved oxygen dynamics. Springer.

Testa, J. M., R. R. Murphy, D. C. Brady, and W. M. Kemp. 2018. Nutrient- and climate-induced shifts in the phenology of linked biogeochemical cycles in a temperate estuary. Front. Mar. Sci. **5**: doi:10.3389/fmars.2018.00114

Tucker, J., A. E. Giblin, C. S. Hopkinson, S. W. Kelsey, and B. L. Howes. 2014. Response of benthic metabolism and nutrient cycling to reductions in wastewater loading to Boston Harbor, USA. Estuar. Coast. Shelf Sci. **151**: 54–68. doi:10.1016/j.ecss.2014.09.018

Wilson, R. E., R. L. Swanson, and H. A. Crowley. 2008. Perspectives on long-term variations in hypoxia conditions in western Long Island Sound. J. Geophys. Res. **113**: C12011. doi:10.1029/2007JC004693

Zehr, J. P., and B. B. Ward. 2002. Nitrogen cycling in the ocean: New perspectives on processes and paradigms. Appl. Environ. Microbiol. **68**: 1015–1024. doi:10.1128/AEM.68.3.1015-1024.2002

Zhang, Q., D. C. Brady, W. R. Boynton, and W. P. Ball. 2015. Long-term trends of nutrients and sediment from the nontidal Chesapeake watershed: An assessment of progress by river and season. JAWRA. **51**: 1534–1555. doi:10.1111/1752-1688.12327

Zhou, Y., D. Scavia, and A. M. Michalak. 2014. Nutrient loading and meteorological conditions explain interannual variability of hypoxia in Chesapeake Bay. Limnol. Oceanogr. **59**: 373–384. doi:10.4319/lo.2014.59.2.0373

Zopfi, J., T. G. Ferdelman, B. B. Jørgensen, A. Teske, and B. Thamdrup. 2001. Influence of water column dynamics on sulfide oxidation and other major biogeochemical processes in the chemocline of Mariager Fjord (Denmark). Mar. Chem. **74**: 29–51. doi:10.1016/S0304-4203(00)00091-8

Acknowledgments

We are grateful to James D. Hagy III for sharing the box-model code that we adapted for this analysis. Support from several grants and contracts have made this research possible, including the US National Science Foundation grants (1) DEB1353766 (OPUS; Kemp and Boynton) and (2) CBET1360415 (Testa and Kemp), (3) US National Oceanic and Atmospheric Administration (NOAA) grant NA15NOS4780184 (Testa and Kemp), and (4) National Aeronautics and Space Administration (NASA) grant NNX14AM37G (Kemp and Testa). We thank Johanna Rambo, Jennifer Humphrey, and Casey Hodgkins for their help with the box-model implementation and data analysis. This is contribution # 5490 from the University of Maryland Center for Environmental Science.

Conflict of Interest

None declared.

Submitted 14 November 2017
Revised 15 March 2018
Accepted 05 April 2018